Tectonophysics 873 (2024) 230214

Contents lists available at ScienceDirect

Tectonophysics

journal homepage: www.elsevier.com/locate/tecto

The NE-SW Sibari fault zone: A seismic hazard source in Ionian Northern Calabria (Italy)

F.R. Cinti [a,*], L. Alfonsi [a], L. Cucci [a], D. Pantosti [a], C. Pauselli [b], M. Ercoli [b], C.A. Brunori [a], G. Cianflone [c], R. Dominici [c]

[a] Istituto Nazionale di Geofisica e Vulcanologia, Roma, Italy
[b] Dipartimento di Fisica e Geologia, Università degli Studi di Perugia, Perugia, Italy
[c] Dipartimento di Biologia, Ecologia e Scienze della Terra (DiBEST), Università della Calabria, Arcavacata di Rende, Cosenza, Italy

ARTICLE INFO

Keywords:
Active faults of Italy
Seismic hazard
Offset streams
Displaced marine terraces
Sybaris archaeological site

ABSTRACT

A multidisciplinary approach including archaeological, geophysical, and geological/geomorphological surveys provided pieces of evidence that allowed us to identify the Sibari fault zone (SFZ) in Northern Calabria (Italy). The SFZ runs in a ~ NE-SW direction for a length of ~18 km from the Ionian coastline to Terranova da Sibari and has an oblique normal-dextral kinematics. The envelope of the SFZ is derived from several direct and indirect evidence resulting in subparallel and locally en-echelon fault traces over a maximum 500 m-wide band, running at different elevations across hills and flat lands. The SFZ was active since at least the Middle-Upper Pleistocene, producing faulting of alluvial deposits, marine terraces, drainage incisions, and the archaeological structures of Sybaris. Given the fault length and assuming a seismogenic behavior, the SFZ is a primary earthquake source possibly producing moderate to large earthquakes ($M \geq 6$). We calculated the average slip rates along the SFZ based on the ages and on the accumulated displacements of offset streams and marine terraces. The estimates are of 0.05–0.18 mm/yr and 0.41–0.70 mm/yr for vertical and dextral slip, respectively. Based on both the measured (min. 30 cm) and the expected value (av. 40 cm) of lateral slip per event, we infer an average recurrence for surface faulting events on the SFZ of about 700–1000 yrs. The most recent surface faulting earthquake occurred on the fault is dated 1300–1100 yrs. ago, highlighting that the elapsed time approaches the estimated average recurrence. Considering these findings, the newly recognized SFZ should be included among the faults that contain a potential seismic hazard in this poorly known portion of the Ionian sector of northern Calabria.

1. Introduction

The Sibari plain in northern Calabria (southern Italy) is located at the boundary of the Southern Apennines with the northeastern Calabrian Arc, in an area critical for the understanding of the seismogenic processes controlled by the NNW-SSE convergence between Eurasia and Africa-Adria continental plates (Fig. 1; Faccenna et al., 2001 and references therein). The geologic, seismologic, and geodetic evidence of tectonic activity (Fig. 1) indicates that extensional and strike-slip tectonics accommodate the deformation of this region (e.g., Van Dijk et al., 2000; Tansi et al., 2007; Del Ben et al., 2008; D'Agostino et al., 2011), however, unlike the Tyrrhenian (western) side of the Calabrian Arc, the seismotectonics of the Ionian sector of the Calabrian peninsula is still not well defined, both in terms of active tectonics and of seismic activity. This is likely because the Ionian sector is characterized by relatively low rates of deformation (D'Agostino et al., 2011) and by a low level of historic and instrumental seismicity (Tertulliani and Cucci, 2014; Rovida et al., 2022). In the Pollino Chain area (north and west of the Sibari Plain, Fig. 1) several active mainly normal faults are recognized (Cinti et al., 1997, 2002; Michetti et al., 1997; Brozzetti et al., 2017a) and moderate seismicity indicates mostly the occurrence of extension (i.e., in 1998 and in 2010–2015 sequences, Fig. 1; Napolitano et al., 2021; Cirillo et al., 2022; De Gori et al., 2022). Conversely, the Sibari plain and its coastal area appear to contain only two NE-SW tectonic lineaments near the Crati River (CRF and TF in Fig. 1 - Lanzafame and Tortorici, 1981), and the E-W normal Rossano Fault (RF in Fig. 1 - Galli et al., 2010). The instrumental seismicity is so limited that it does not allow the recognition of any specific trend that could lead to the imaging of these faults at depth. According to Galli et al. (2010) the Rossano fault is possibly the source of the 1836 event. Farther offshore in the Ionian Sea,

* Correspondig author.
E-mail address: francesca.cinti@ingv.it (F.R. Cinti).

https://doi.org/10.1016/j.tecto.2024.230214
Received 9 October 2023; Received in revised form 21 December 2023; Accepted 14 January 2024
Available online 16 January 2024

the focal mechanisms of the instrumental seismicity and reflection seismic profiles (Fig. 1 and references therein) suggest compressive and strike-slip tectonic regime.

In this context, we have to consider the fact that the Sibari plain area, although with low strain rates, may have experienced strong earthquakes with recurrence times exceeding the temporal coverage of historical and instrumental seismic catalogs. Indeed, several studies based on different research approaches suggest that the area should have experienced damaging earthquakes in the past (e.g., Ferranti et al., 2019; Kagan et al., 2017; Galli et al., 2010; Cinti et al., 2002, 2015a and references therein). All that translates to a potential seismic hazard of this region and to a related high seismic risk, especially along the coastal strip hosting residential areas and critical infrastructures (e.g., refineries, power plants, harbors).

In this work, we focus our efforts on the understanding of the NE-SW Sibari Fault Zone (hereinafter referred to as SFZ), firstly defined by Cinti et al. (2015a), and on its possible extension across the Sibari plain and bounding hills. Based on archaeoseismological studies carried out at the ancient *Sybaris* settlement, Cinti et al. (2015a) (Figs. 1 and 2) define the SFZ as an active, oblique fault zone with a normal-dextral component that ruptured during the past ~2000 yrs.

In the following, we present new multidisciplinary data that, once integrated, allow us to better trace the SFZ and characterize its activity. We collected new archaeoseismic and geophysical data in and around the *Sybaris* archaeological area (Zone 1 in Fig. 2), new morphotectonic data in a small area near Terranova da Sibari (Zone 2 in Fig. 2) and analyzed fluvial and coastal systems (drainage pattern, marine terraces) in a wide area of the plain and bounding hills (Zone 3 in Fig. 2).

2. The Sibari fault zone

The SFZ is an oblique dextral-extentional, 45°-55°-striking fault zone firstly recognized by Cinti et al. (2015a) on the basis of archaeoseismological studies at the *Sybaris* settlement, near the Crati River mouth (Figs. 1 and 2). Here, the activity of the SFZ is recorded by the brittle deformation and damage of seismic origin (fractures, faults, liquefaction, rotations of walls, warping, and collapse) of walls and pavements of the Roman Town (Fig. 3). The fault zone is composed of subparallel cracks observable for a length of about 1 km in a max 80 m-wide area (Fig. 3, and see extended description in Cinti et al., 2015a), mostly showing opening of max 5 cm and, locally a right-lateral sense of movement up to 30 cm. Based on the archaeological stratigraphy and absolute dating of sediments and ceramic shards, Cinti et al. (2015a) recognize two distinct events of faulting affecting the site in the past 2 kyrs B.P. The older event occurred after about 150 CE (no upper limit given) and produced widespread collapse within the whole area of Casa Bianca (see Fig. 3 for location). The second earthquake, dated around 685–885 CE, was identified by an intense fracturing and liquefaction phenomena in the whole area. The high sedimentation rate during Pleistocene and Holocene times due to the active subsidence (Cucci, 2005; Ferranti et al., 2011; Cianflone et al., 2015; Amoroso et al., 2023) that characterizes the flat Sibari plain, has deeply buried and hidden the

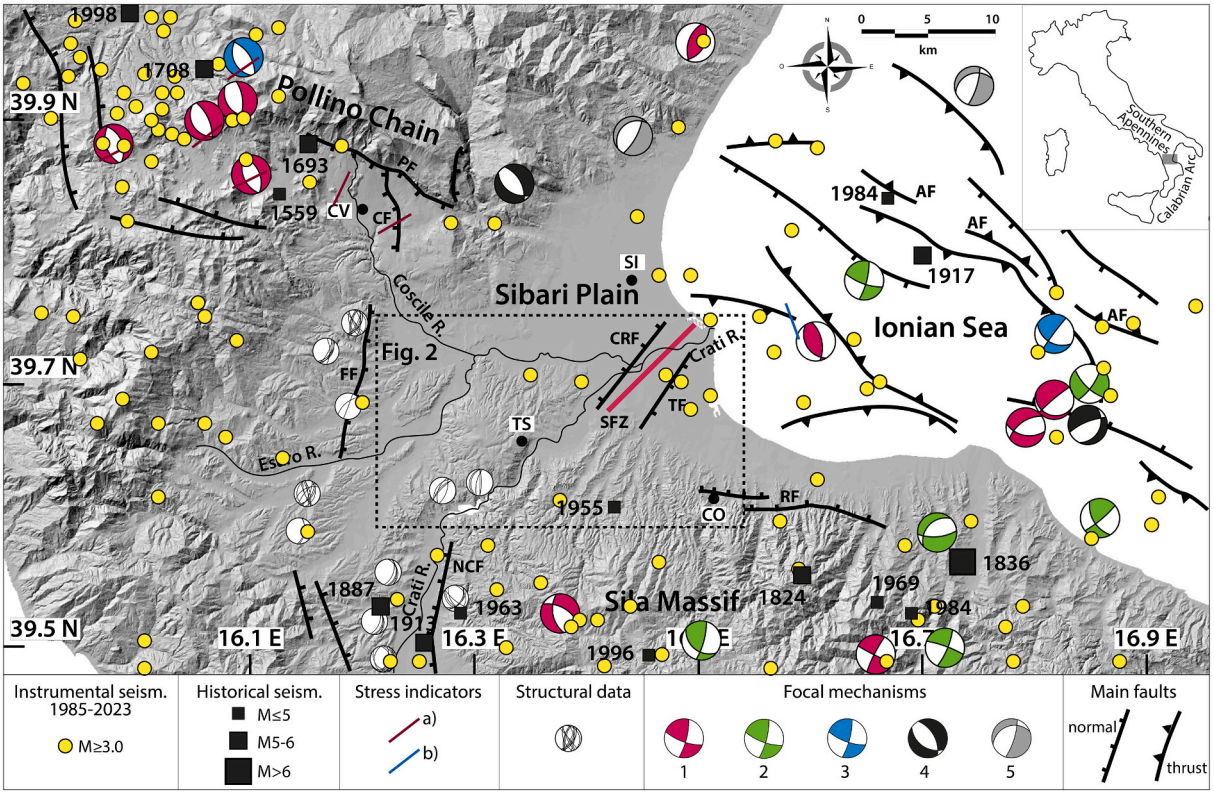

Fig. 1. Seismotectonic map of Northeastern Calabria and location of the Sibari fault zone (SFZ, red line) as inferred in Cinti et al. (2015a). Symbols: yellow circles indicate M ≥ 3.0 earthquakes occurred between January 1985 and December 2023 (ISIDe Working Group, 2007). Focal mechanisms (see Table S1 in the Supporting Material for earthquake parameters of the focal mechanisms): 1 - TDMT (Scognamiglio et al., 2006); 2 - EMMA Database (Vannucci and Gasperini, 2004); 3 - CMT Dataset (Pondrelli et al., 2006); 4 - Frepoli et al., 2011; 5 - Frepoli and Amato, 2000. Historical seismicity (black squares) is from the Italian Seismic Catalogue (Rovida et al., 2022). Stress indicators (Shmin orientation from active faults and focal mechanisms) from the IPSI Database (Mariucci and Montone, 2022): a) normal faulting; b) thrust faulting. Structural data from Brozzetti et al. (2017b). Faults modified after Brozzetti et al. (2017a), Cinti et al. (1997, 2002, 2015a), Del Ben et al. (2008), Ferranti et al. (2014), Galli et al. (2010), Lanzafame and Tortorici (1981), Michetti et al. (1997), Quye-Sawyer et al. (2021). Abbreviations for main faults: AF - Amendolara Fault, CF - Castrovillari Fault, CRF - Crati Fault, FF - Firmo Fault, NCF - North Crati Fault, PF - Pollino Fault, RF - Rossano Fault, TF - Timparelle Fault. Abbreviations for towns: CV - Castrovillari, SI - Sibari, TS - Terranova da Sibari, CO - Corigliano Calabro. The dashed rectangle indicates the area shown in Fig. 2. (For interpretation of the references to colour in this figure legend, the reader is referred to the web version of this article.)

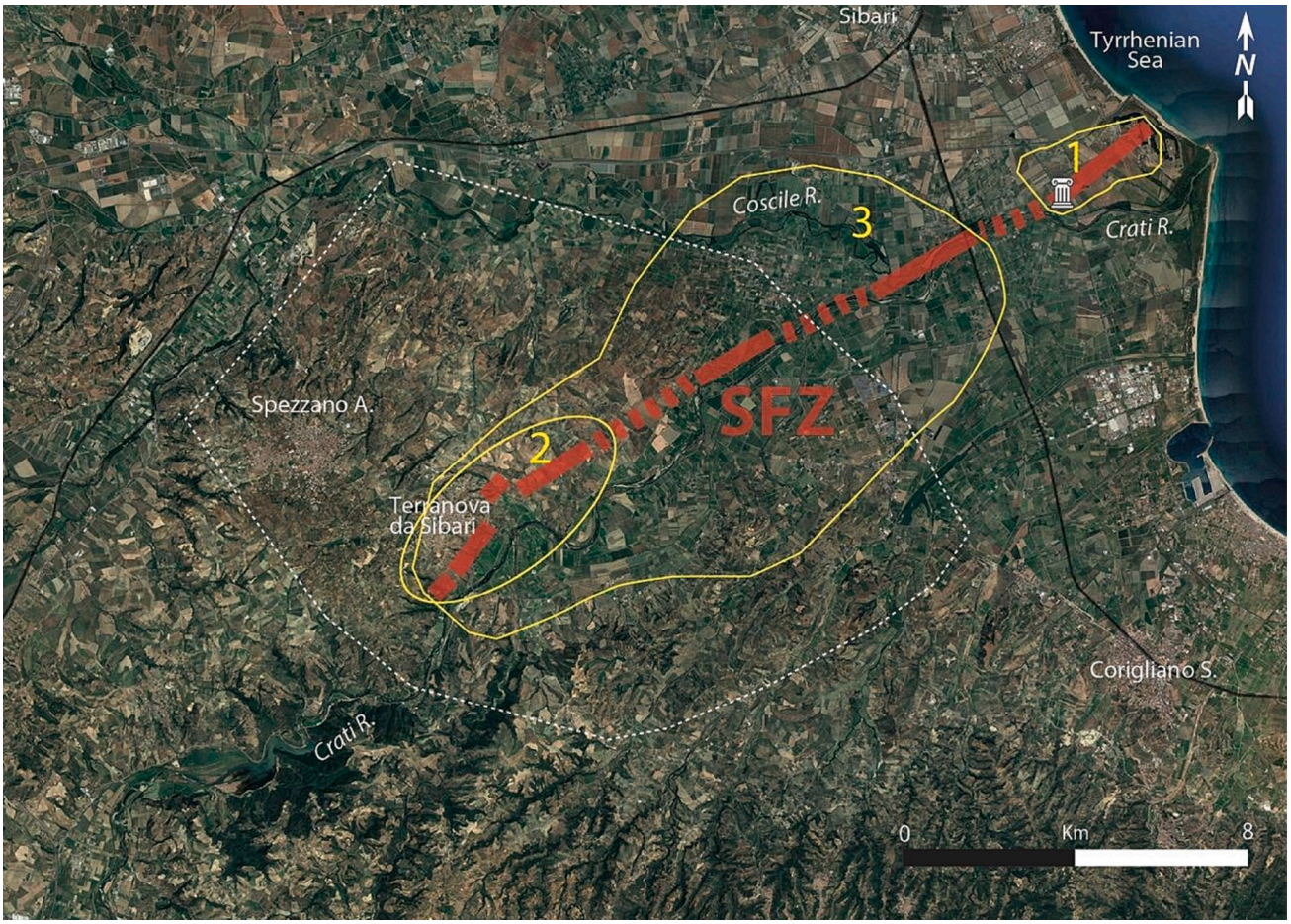

Fig. 2. The Sibari fault zone (red bands) investigated by means of different approaches, from archaeoseismology and geophysical prospecting to morphotectonics. The three zones enclosed in the yellow lines (1,2,3) represent the study areas as discussed in the text; the column (in zone 1) indicates the location of the ancient settlement of *Sybaris*; the dashed white line encloses the marine terrace mapping area from Alfonsi et al. (2023). Satellite image from Google Earth © Map. (For interpretation of the references to colour in this figure legend, the reader is referred to the web version of this article.)

SFZ at the surface preventing the recognition of any direct evidence for the fault away from the excavation of the archaeological site. However, indirect data suggests that the NE-SW trending fault zone likely extends northeast and southwest outside of the archaeological site. Based on the analysis of elevation profiles and anomalies of riverbeds just SW of the site, Cinti et al. (2015a) suggest that the SFZ is dismantling a 2-3 m-high structural relief bordered by the NE-SW striking Crati and Timparelle faults (CRF and TF in Fig. 1; Lanzafame and Tortorici, 1981; see also Fig. 5a and b in Cinti et al., 2015a). The structural relief served as a drainage boundary between the Crati and Coscile paleorivers, and then controlled the recent local morphology and the present Crati River course.

Also, Cianflone et al. (2018), combining borehole data and ERT (Electrical Resistivity Tomography) profiles at different locations, suggest that the present stratigraphic pattern of the plain can be related to the late Quaternary activity of a NE-SW normal-dextral fault zone, i.e., the SFZ. In fact, the ERT data collected near the coastline about 1.5 km NE of the *Sybaris* site enhance a high and sharp resistivity vertical contrast in the subsurface (Fig. 4). This anomaly is interpreted as the subsurface signature of a fault zone that would be compatible with the prolongation to the ENE of the SFZ imaged at the archaeological site (Fig. 3). In addition, Cianflone et al. (2018) identify areas characterized by groundwaters with high electrical conductivity and Cl contents and hypothesize the presence of plumes of deep mineralized waters which use the tectonic discontinuities to rise toward the surface.

However, the limited knowledge about the SFZ observed so far in a localized area near the coast, leaves several open questions about its relevance in the area, its extent and rates of activity, and whether the SFZ is a primary earthquake source or, alternatively, a secondary fault that slips to accommodate the coseismic deformation from faulting on a different structure (Cinti et al., 2015a).

With the aim of exploring the whole extent of the SFZ, understanding its kinematics, and rates of activity, we started new multidisciplinary investigations and collected new data in an elongated area between the archaeological site of *Sybaris* and the Terranova da Sibari village (Fig. 2).

3. New data

During the past years we collected and analyzed new archaeoseismological, geophysical, and geologic/geomorphic data to better define the SFZ. The geologic/geomorphic data comprise the analysis of the landscape of well-preserved flights of uplifted marine terraces, the drainage network, the hills morphology, and the tectonic features.

Our analysis mainly focuses on a broad band extending from the ancient site of *Sybaris* to the village of Terranova da Sibari, and was developed both at local and wide scales. In the following, we are going to present data and results from the three zones depicted in Fig. 2: zone 1, the archaeological site of *Sybaris*; zone 2, the hills of Terranova da Sibari; zone 3, the broad NE-SW upper Crati River area between zones 1 and 2.

3.1. *Sybaris archaeological site - ZONE 1*

3.1.1. *Archaeoseismic evidence*

We conducted the archeoseismic survey on ruins that were newly

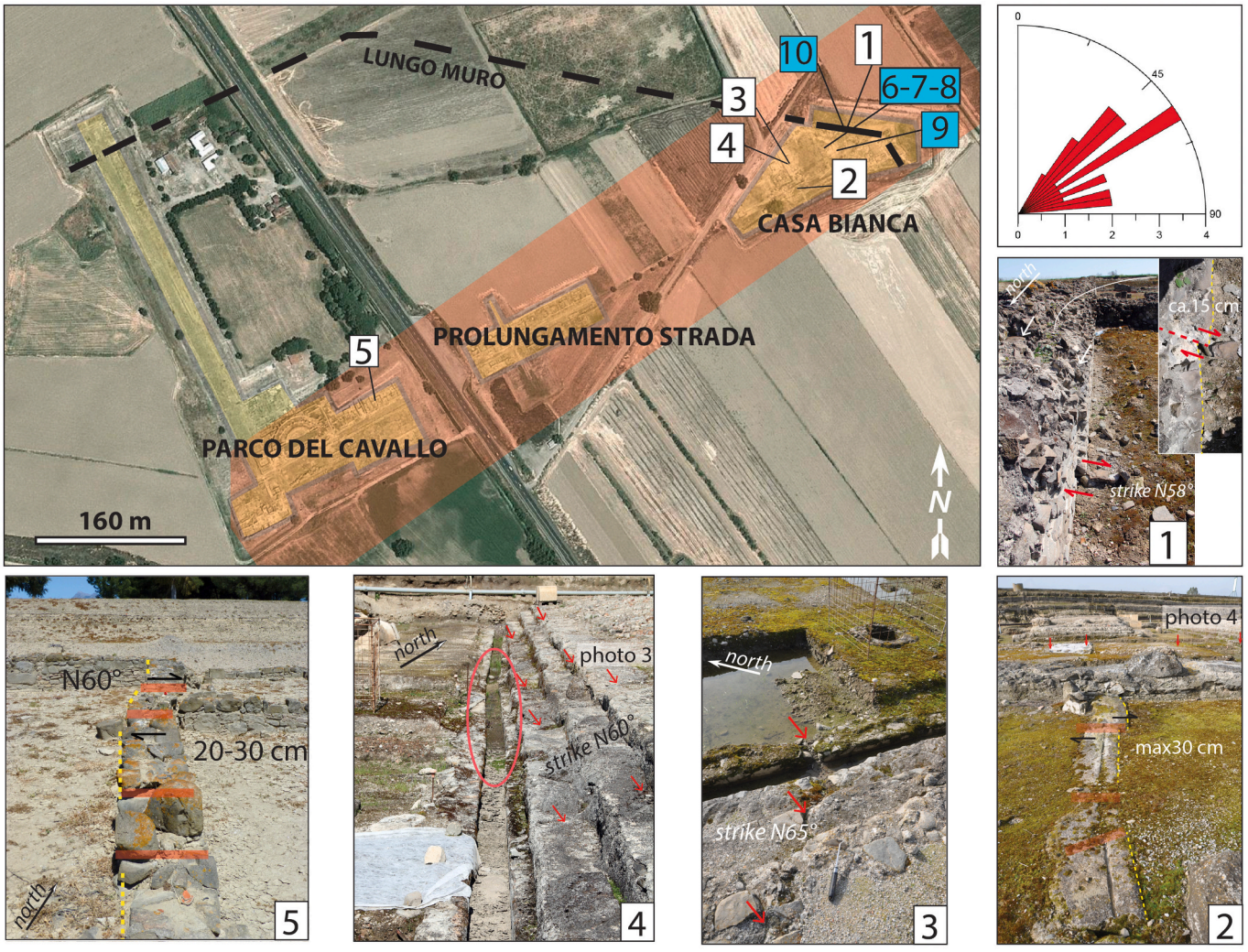

Fig. 3. Upper left: aerial view of the archaeological excavations of *Sybaris* from Google Earth © Map. The red band highlights the SFZ deformation zone according to Cinti et al. (2015a). White numbered boxes indicate the location of the photos (1 to 5) that show some of the tectonic brittle deformation reported by Cinti et al., 2015a; these are laterally shifted walls (1, 5), fractured steps, pavements and porticos (2, 3, 4), and distortion of a conduit for sewage disposal (4). Blue numbered boxes (6 to 10) refer to new observations; photos are shown in Fig. 5. Upper right: rose diagram showing the strike of the SFZ fractures. (For interpretation of the references to colour in this figure legend, the reader is referred to the web version of this article.)

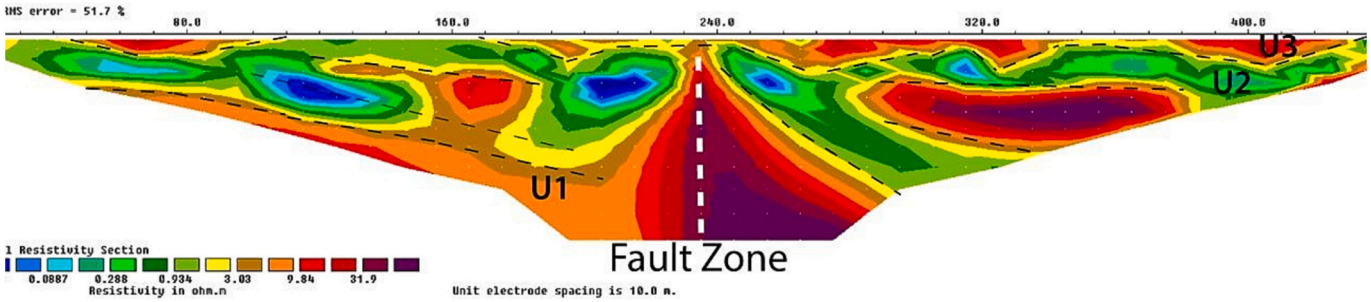

Fig. 4. Inverted ERT section (ERT max depth ~ 100 m) and its interpretation modified from Fig. 10, ERT 20 in Cianflone et al. (2018). Location of the section is near the coastline about 1.5 km NE of the Sybaris site. The section shows a sharp lateral resistivity contrast in the subsurface interpreted as the signature of the fault zone (white line). Stratigraphic interpretation of the resistivity layers (separated by black lines): U1: alluvial and coastal plain deposits (Late Pleistocene); U2: clayey deposits of marine-marshy-lagoon origin (early-middle Holocene); U3: coastal (at the bottom) and deltaic sediments (middle-late Holocene).

exposed in the 2014 excavations by Greco (2017), and not included in the survey by Cinti et al. (2015a). These excavations revealed new features of faulting and liquefaction significantly deforming and rupturing an area of the northern sector of the Roman ruins at Casa Bianca (Fig. 3). We surveyed the brittle deformation expressed as broken and collapsed pavements and roofings, fractured and deformed walls that also appear burst and dismantled by pervasive fissures and fractures with injection of liquefied sand (Fig. 5). The fractures occur within the bands of deformation previously inferred and are consistently oriented with the 45°-55°-striking coseismic brittle zone, i.e., the fault zone

Fig. 5. Brittle deformation observed during the new survey at the *Sybaris* site. Photos 6–7-8: main open fracture with the injection of liquefied sand dissecting the Roman remains; photos 9–10: fractured walls, pavements, and collapses. Photo location: blue numbered boxes in Fig. 3. (For interpretation of the references to colour in this figure legend, the reader is referred to the web version of this article.)

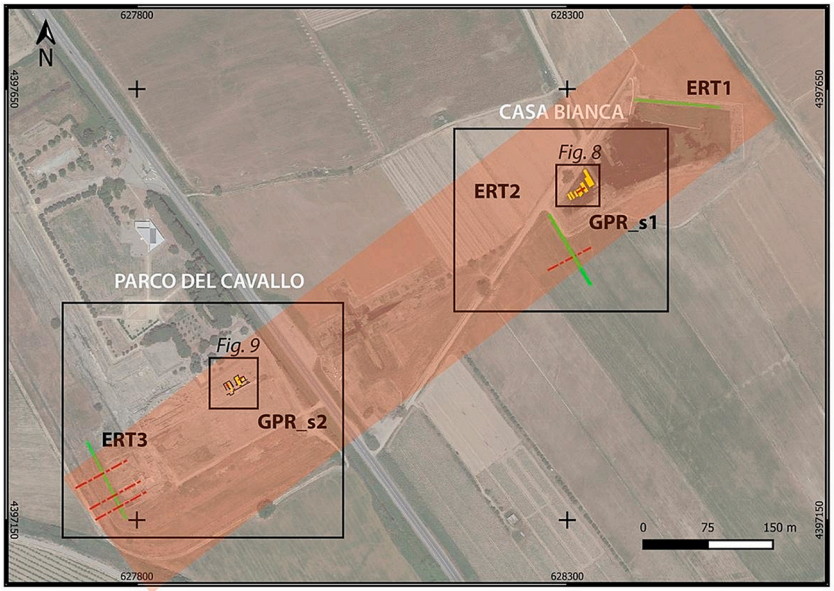

Fig. 6. Geophysical data collected at the ancient *Sybaris* site (zone 1) across the SFZ (light red band). Two main areas were surveyed (large black boxes), Casa Bianca and Parco del Cavallo. The green lines represent the ERT profiles: ERT1, ERT2, ERT3. Small black boxes named GPR_s1 and GPR_s2 were surveyed using 2D and 3D GPR profiling (yellow lines). The red dashed lines represent the location of the subvertical discontinuities recognized in the ERT profiles (details in Fig. 7). (For interpretation of the references to colour in this figure legend, the reader is referred to the web version of this article.)

(Fig. 3). Where observed, the opening of fractures reaches 6–7 cm, both on soil and structures (photos 7 and 9 in Fig. 5). Some man-made structures appear also horizontally displaced (a few cm), confirming the right-lateral motion previously observed. Indeed, the location, geometry (alignment, strike), and kinematic (opening, slip direction) of the newly revealed coseismic features are in agreement with those reported by Cinti et al. (2015a) and provide a strengthened picture of the subparallel bands of fractures (Fig. 3; see also chapter 2).

Given the availability of the stratigraphy from a 20 m-deep borehole drilled within the settlement area (Stanley and Bernasconi, 2009), we infer that the liquefied sand filling the open fissures (photos 7 and 8 in Fig. 5) could have the source bed located at about 8–9 m of depth.

Radiocarbon analysis confirms that the observed fracturing and paleoliquefaction are associated with the occurrence of the youngest of

the two paleoearthquakes recognized at the site by Cinti et al. (2015a). Dating of the fractured soil newly exposed by the excavation allows us to also constrain the *post quem* age of this event to 655–765 CE (photo 7 in Fig. 5). Integrating this age with the age from Cinti et al. (2015a) from undeformed organic alluvium (685–885 CE) and considering the archaeological stratigraphy, we set the most recent paleoearthquake occurrence at around 1300–1100 yrs. B.P.

The new observations on the deformation/ruptures/coseismic effects of the built structures from the *Sybaris* site strengthen the presence of a continuous NE-SW faulting zone crossing the settlement and cutting different types of manmade structures and soil. These observations imply high-intensity earthquake shaking at the site and suggest a minimum magnitude equal to or larger than 5.5.

3.1.2. Geophysical evidence

Integration of Electrical Resistivity Tomography (ERT) and Ground Penetrating Radar (GPR) data with geologic and archaeoseismic data is used to investigate the SFZ at the *Sybaris* site and its inferred prolongation in the recent sedimentary deposits nearby. Three ERT sections, each 99 m long (ERT1, ERT2, and ERT3), were acquired using 100 electrodes and 1 m spacing and Pole-Dipole, Dipole-Dipole and Wenner configurations (Ercoli et al., 2012; Cinti et al., 2015b) at the sides of the remains of the archaeological area and near the masonry remains areas (Fig. 6). These allowed us to reach investigation depths up to ~20 m (Fig. 7). Details on the data processing applied are provided in S2 in the Supporting Material.

The ERT2 and ERT3 resistivity pseudo-sections, the starting models, and the inverted Wenner ERT sections are displayed in Fig. 7 (the ERT1 line is not shown due to the lack of clear lateral resistivity variations interpretable as geological discontinuities).

The inverted sections ERT2 and ERT3 (Fig. 7) show that the sedimentary deposits in the subsurface at the archaeological site have average values of resistivity mostly below 100 Ωm, comparable among the different locations. The sections clearly show horizontal resistivity contrasts up to the max depths, suggesting stratigraphic variations associated with alternances of alluvial sediments: the latter are lenses of gravel and sand (higher resistivity, 20–40 Ωm), and clay layers (lower resistivity, below 20 Ωm). This stratigraphy is interpreted as the result of ephemeral channeling during exceptional floods. At least one clear, sharp variation of the resistivity values is detected in ERT2 whereas three are detected in ERT3 (red dashed lines in Fig. 7 and map location in Fig. 6). Although these vertical and sharp anomalies show relatively limited resistivity variations associated with the different lithologies, they have a good continuity at depth.

Such discontinuities are aligned in a zone ~50 m wide and in agreement with the NE-SW orientation of the fractured zone mapped by the archaeoseismic survey (Fig. 6; see also chapters 2 and 3.1.2). This strengthens the link between the shallow subsurface and surface evidence of the SFZ. Also, the location of the ERT anomalies presented here fits with that recognized in some of the ERT sections reported by Cianflone et al. (2018). These latter, acquired at a larger scale, show similar sharp lateral resistivity variations up to depths of 100 m. Despite the different scales and resolutions of acquisition, the shallower portions have values of resistivity and horizontal setting comparable to these results.

The GPR surveys were carried on the floor of the excavated archaeological structures and close to the faulted fractured masonries at a more detailed scale than ERT (Fig. 6). The artificial cover in the site (thick spoil and textiles sheets in places), the possible presence of buried manufacts, and also the high conductivity of the surveyed media, lead to a relatively low GPR signal penetration, for a maximum investigation depth of ~1.5 m.

At the GPR_s1 site, we have collected n.18 GPR profiles (Fig. 8) using a Radsys Zond 12e GPR system, equipped with two antennas of central frequency 500 and 1500 MHz. We used a time window ≤100 ns, 512 samples for each trace and a trace spacing of 1 cm, measured by a survey wheel; additionally, n.8 GPR profiles spaced 0.5 m were used to collect a pseudo-3D GPR cube, focused where the alignment of fractures filled by liquefied sand was visible at the surface (green area in Fig. 8b). The conventional GPR processing workflow was applied, and it is reported in Table S2 in the Supporting Material. A clear lateral interruption (phase discontinuity) of the GPR reflections and sharp decrease in the GPR signal amplitude (localized attenuation), together with a small hyperbolic diffraction (enclosed in white boxes in Fig. 8c, d), are observed across the fracture filled with liquefied sand.

At the GPR_s2 site, we recorded n.4 GPR profiles using a 500 MHz antenna close to the displaced walls (Fig. 9a, b); the trace spacing was again set up to 1 cm, the time window 100 ns and the samples/trace were 512. The pseudo-3D GPR volume, which is 4.5 m × 4.5 m long, was recorded using a profile spacing of 10 cm. Within the same survey area, n.16 GPR profiles, spaced 30 cm, were also collected using a 1500 MHz and a time window of 25 ns. The GPR processing workflow is shown in Table S2 in the Supporting Material. The GPR profiles close and parallel to the laterally offset walls (Fig. 9b) show diffractions and subvertical discontinuity likely marking the presence of the fractures at shallow depth in continuity with the ones visible across the walls at the surface (Fig. 9c). A better visualization of the fractures is definitely presented on the 3D GPR volume also using time-slices such as in Fig. 9d.

3.2. The hills of Terranova da Sibari - ZONE 2

3.2.1. Local anomalies in the streams' course

Abrupt deflections of stream channels running on the steep slopes south of Terranova da Sibari are found (Fig. 10). These streams are tributaries of the Crati River and cut the bedrock forming narrow and deep V-shaped valleys until they reach the basal river level.

These valleys show abrupt dextral lateral shifts (Fig. 11), that we interpret as due to cumulative horizontal tectonic slip along the SFZ. In correspondence of these sharp deflections, we found fault planes and joints (see chapter 3.2.2), knick-points, internal channels, waterfalls, and potholes, shutter ridges, and, at places, also the former beheaded courses of the channels (Fig. 11). All these characteristics indicate the vicinity of the displacement zone, i.e. of the fault line (Fig. 11) and also point to a vertical component of the displacement (e.g., knick-points, waterfalls). This vertical component would produce a SE lowering yielding an oblique dextral movement on the SFZ. It is worth noting that there are no changes in lithology or specific morphologies that can explain these features.

Repeated movements through time on the SFZ lead to the development of a typical morphology of the drainages with: 1. the shutter ridges obstructing the channels producing deceleration of the erosion upstream with formation of potholes and deposition of loose sand, 2. the convergence of internal channels at the knick-points, and 3. a clear vertical separation of the planar stream bottom at the knick-points (Fig. 12).

Fig. 12 also shows the typical headward erosion of the downstream channel clearly related to the interaction between the tectonic motion and the relative lowering of the basal level (i.e., Crati River); as a consequence, the stream is strongly incised and joins the Crati River in a short distance.

Lateral offset measurements of the stream channels were performed by reconstructing the talweg geometry assuming an initial quasi-rectilinear geometry. The average trend of the talweg was projected into the fault zone yielding lateral offsets ranging from 80.3 to 86.5 m (Fig. 13). These values represent the average of the measurements taken assuming different projections of the talweg across the fault zone; they are representative also of the other stream deflections along the slope.

Projecting the planar and regular bottom of the talweg as appears in the profile of Fig. 12, we can estimate a vertical component of the offset ranging between 10 and 20 m, depending on the talweg bottom projection.

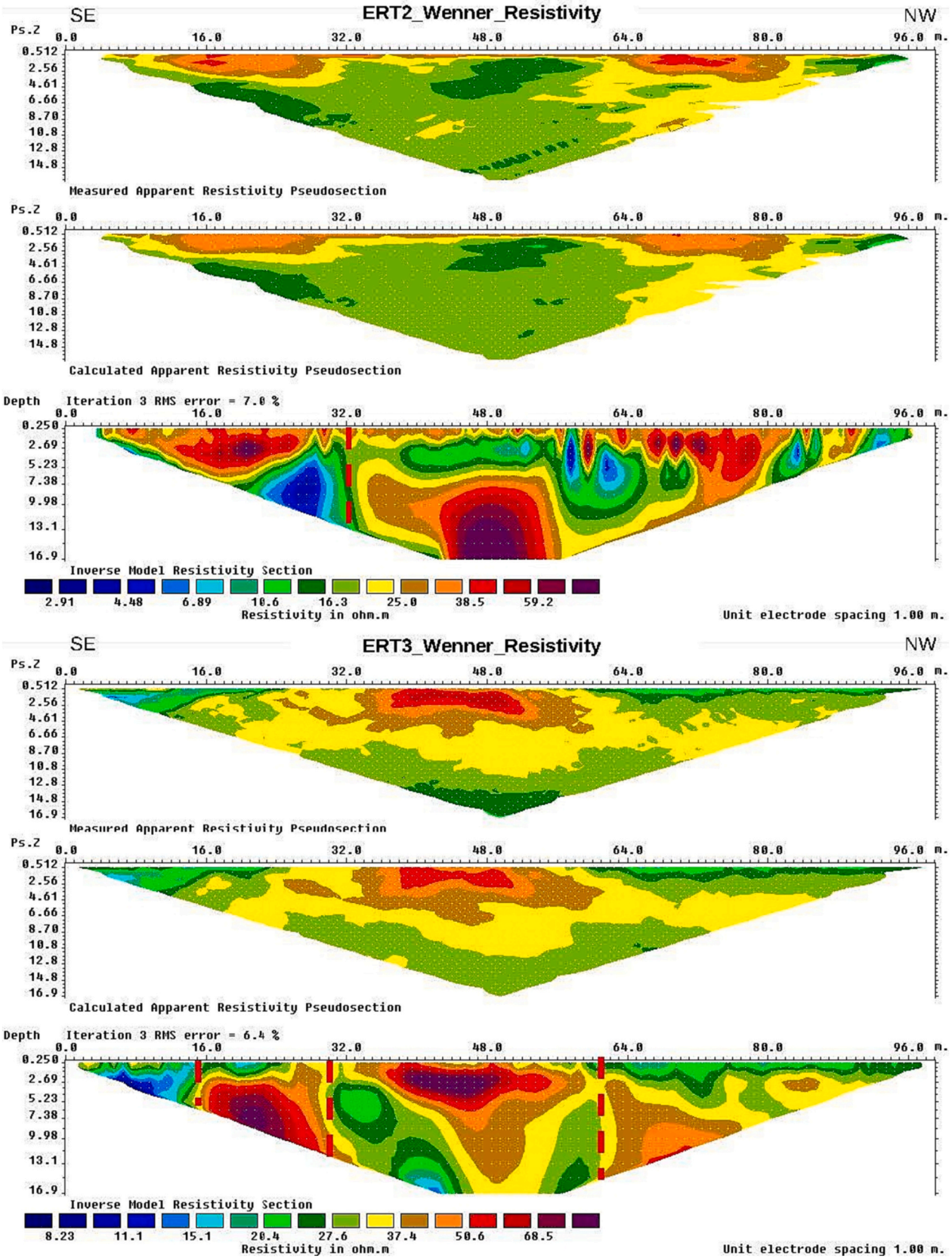

Fig. 7. Results of the ERT2 and ERT3 prospection, respectively, including for each one (from top to bottom) the resistivity pseudo-sections (Wenner configuration), the calculated ones, and the inverted sections. The latter include the relative interpretation of tectonic discontinuities (red dashed lines). (For interpretation of the references to colour in this figure legend, the reader is referred to the web version of this article.)

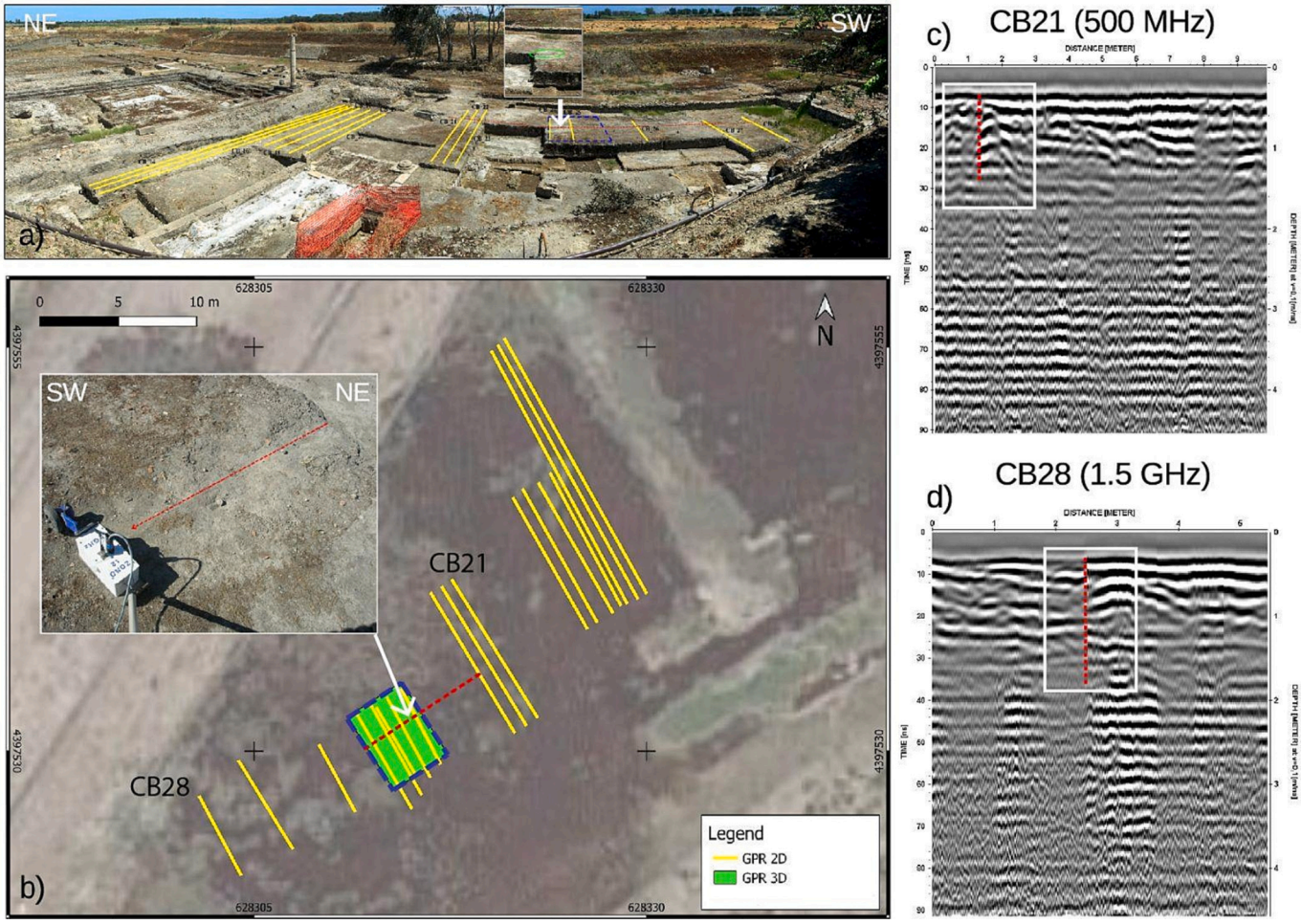

Fig. 8. GPR_s1 site: a) panoramic view of the Casa Bianca site (see Fig. 6 for location), the yellow lines locate GPR profiles, the arrow locates the fracture; b) map view of all the 2D GPR profiles (yellow lines) and of the pseudo-3D GPR data (green polygon), red dashed line is the signature imaged by the GPR and coinciding with the fracture at the surface; c, d) interpreted profiles CB21 and CB28, the GPR subsurface signature of the sand liquefaction fracture (red line within the white box) is represented by hyperbolic diffractions, lateral phase discontinuities, and amplitude variation of the reflections. (For interpretation of the references to colour in this figure legend, the reader is referred to the web version of this article.)

3.2.2. *Field fault recognition*

Limited outcrops, steep slopes, and thick bushy vegetation make it difficult the direct observation of tectonic features in the study area. Some sub-vertical fault planes and fissures are observed at different locations in correspondence of the channel deflections but cannot be followed outside the incisions with exception of saddle changes in slope (photo 2 of Fig. 11). The few small planes that could be measured have a quite homogeneous strike of N30°-45° and sub-vertical dip. These planes cut across bedrock units (schists and phyllades of Giurassic-Cretaceous age), and in one case cut cemented marine sands of Pleistocene age. Moreover, waterfalls, knick-points, potholes, and displaced marine terraces (see chapter 3.3.2) indicate young displacements along these faults.

Interestingly, a huge travertine deposit covering a cliff and some minor blocks outcrop in alignment with the offset streams to the southwest (see chapter 3.2.1 and yellow dots in Fig. 10). These are interpreted as additional evidence of the SFZ.

Further north-east, faulted young deposits are found at the Grotte site on the steep SW edge of the "Varco del Lupo" stream valley (Fig. 10 for location). Here, the fault zone puts in subvertical contact Lower Pleistocene marine deposits with continental conglomerates and colluvium (photos 7 and 8 of Fig. 11). The fault zone is characterized by highly sheared and verticalized pebbles; vertical fault planes are oriented N25°-45°, with uncertainty due to the difficult access for unstable terrain on the cliff. Despite the area being highly modified by agricultural activities and constructions, additional evidence for active faulting near the Grotte site is suggested by scarps crossing the young deposits of the valley. The northern scarp forms a bench that is connected with a dextral stream deflection and knick point, as also observed in the deflected channel to the south (yellow dot#3 in Fig. 10).

These pieces of evidence of active faulting, when seen at a broad scale, appear to be arranged in a left stepping en-echelon setting (Fig. 10) whose envelope images a NE-SW zone of deformation, i.e. the SFZ.

3.3. *Upper Crati river valley - ZONE 3*

3.3.1. *Anomalies in the drainage pattern*

Landscape responses to active tectonics occur also at a wide scale and impact drainage patterns producing anomalies that may represent clues for the understanding of the tectonic deformation.

The map of Fig. 14 shows the present setting of the river network of the central Sibari plain along with the abandoned river courses. The map outlines the migration of the Coscile and Crati Rivers to the south and to the north, respectively, to reach the present point of convergence (see star in Fig. 14). Changes in the course of the Crati and Coscile Rivers are well documented in historical reports and maps (Zecchi et al., 2003; Cucci, 2005; Lena et al., 2021). The two rivers underwent repeated

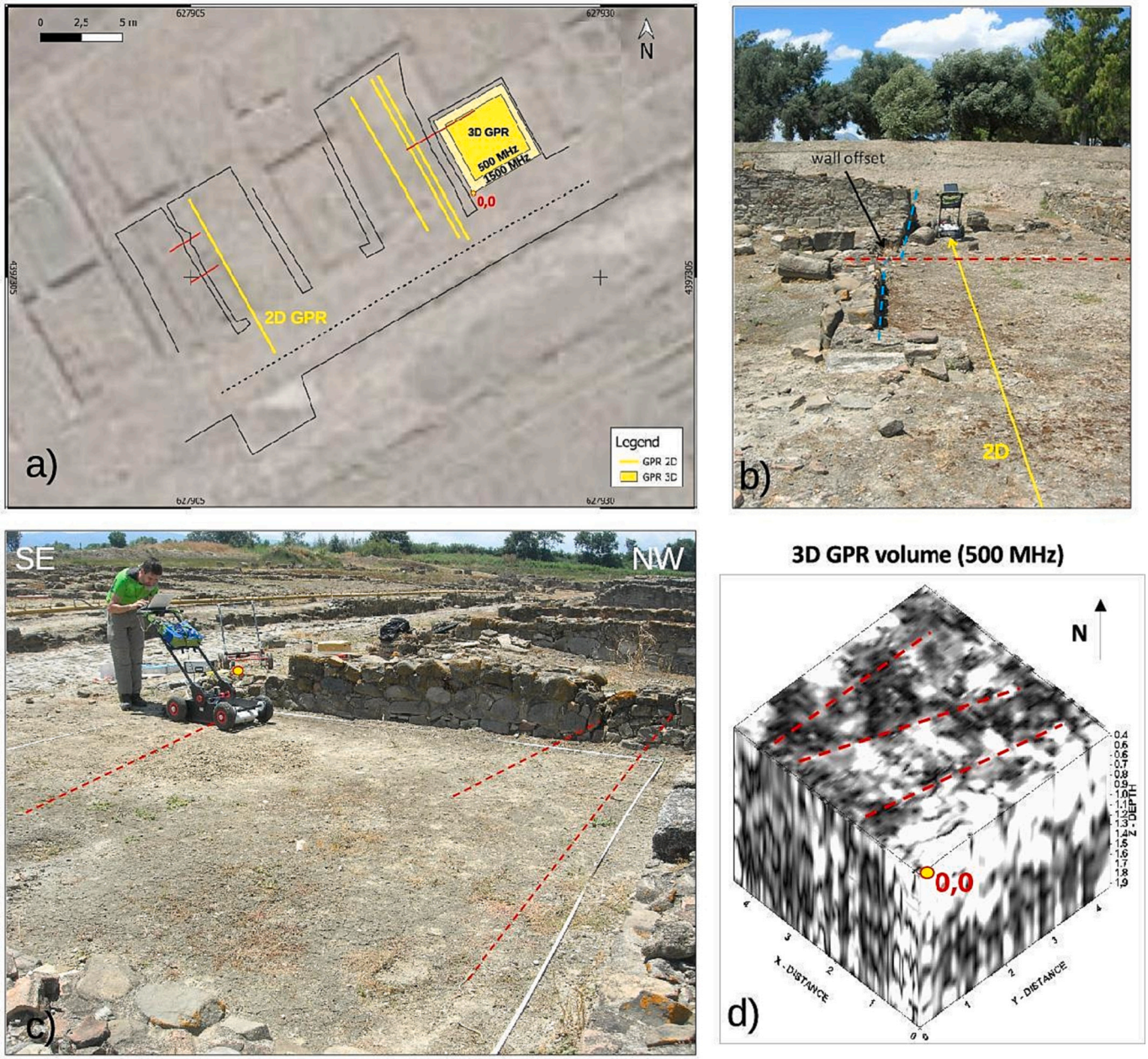

Fig. 9. GPR_s2 site: a) map view of the GPR acquisitions (yellow lines and box); b) detail of the offset wall (blue dashed lines) cut by a fault splay (red dashed line); the yellow line indicates the location of one of the 2D GPR profile; c) location of the 3D cube (yellow dot near the instrument is the 0;0 origin of the local system of coordinates referred to the north, defining the inline (X) and crossline (Y) directions of the GPR grid). The red dashed lines represent the continuation of the fractures cutting and displacing the walls; d) georeferenced dense 3D GPR volume (yellow dot is the 0;0 coordinate); the red dashed lines are the deep GPR signature of the fractures visible at the surface and interpreted using a GPR time-slice 0.4 m deep. (For interpretation of the references to colour in this figure legend, the reader is referred to the web version of this article.)

events of confluence and separation along their path toward the Ionian Sea; historical maps show two separate courses until the end of the 18th Century (Rizzi Zannoni, 1808). The progressive migration of the two main paleo-riverbeds (especially relevant for the Coscile) toward the central part of the Sibari plain can be seen as the result of the activity of the SFZ leading to the lowering of the valley depocenter both because of the vertical component lowering the SE block, and of apparent vertical juxtaposition due to horizontal movement (Fig. 14). Important subsidence of this part of the valley is well expressed by the intense alluviation of the ancient *Sybaris* site; the relevant subsidence is due not only because of sediment compaction and gravity load which is common everywhere in the plain (Cucci, 2005; Ferranti et al., 2011; Cianflone et al., 2018), but likely because of tectonics.

Between Doria and Terranova da Sibari, most of the drainage runs straight N-NE toward the Coscile River, whilst E and NE of Terranova the streams become tributaries of the Crati River and flow to the SE (Fig. 14). The watershed between these two systems runs in a NE-SW direction just north of Terranova da Sibari (dotted line in Fig. 14). The streams indicated as ‘a’ and ‘b’ in Fig. 14 have their upstream course parallel to the watershed and, incidentally, parallel to the SFZ; this is a clear anomaly in the drainage pattern near the fault zone. Moreover, streams ‘a’ and ‘b’ flow along the same axis and are well aligned with some remnants of gullies suggesting that they were part of the same stream course (black line in Fig. 14). Its upstream (‘a’ in Fig. 14) would have been captured (sharp turn ~90°) likely because of the SFZ activity producing an oblique dextral displacement SE side down. Whereas its

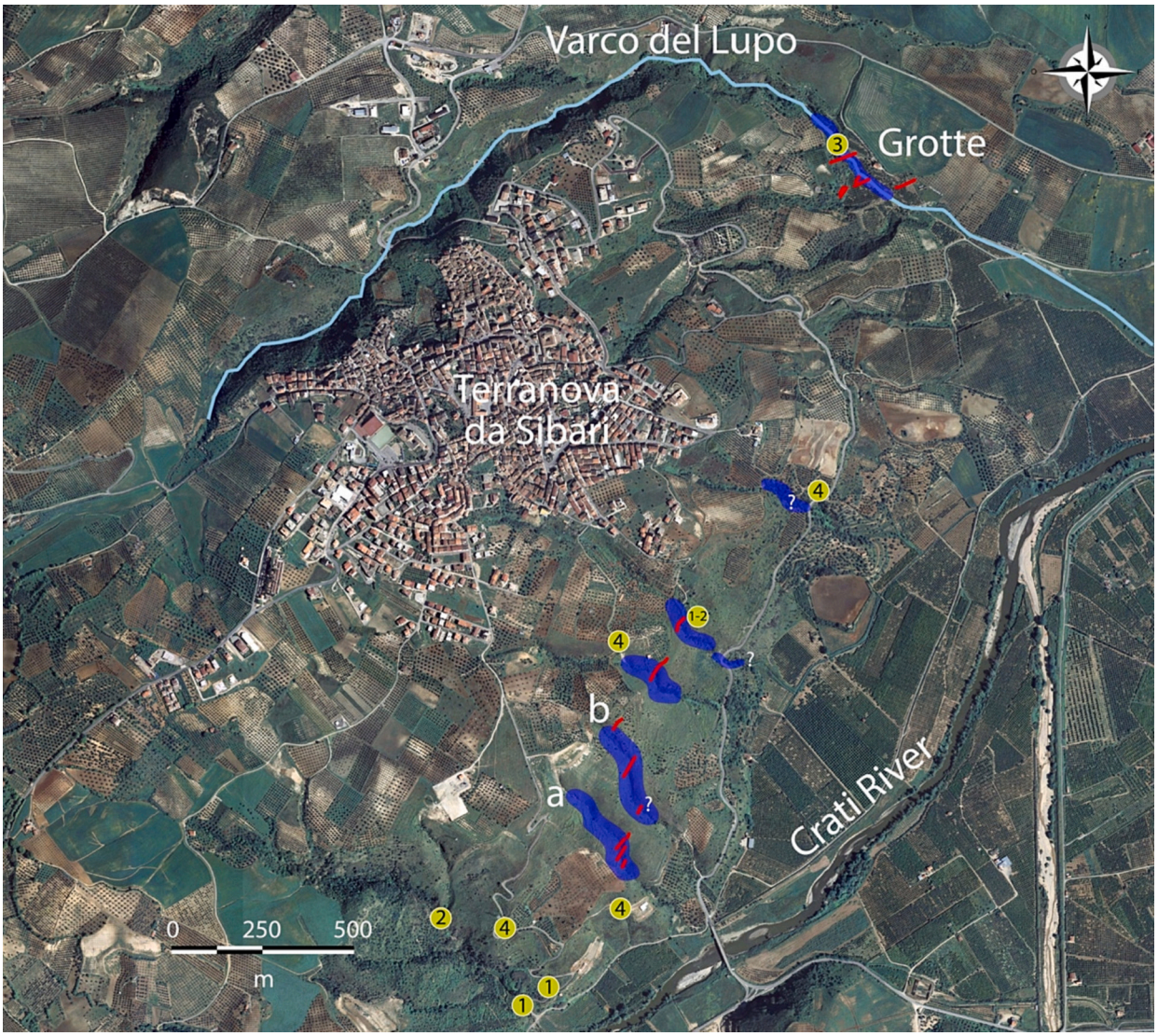

Fig. 10. Map of zone 2 around the village of Terranova da Sibari. Orthophoto from Regione Calabria http://geoportale.regione.calabria.it/. Red lines indicate the fault traces and the morphological scarps mapped during the field survey. Blue shaded areas indicate the deflected stream valleys. Question marks when data is uncertain. Yellow dots enclosing numbers locate other indicators of potential faulting: (1) travertine outcrops, (2) waterfalls, (3) knick points, (4) subvertical contacts bedrock-colluvium (see also photos in Fig. 11). Letters 'a' and 'b' refer to the streams detailed in Fig. 13. (For interpretation of the references to colour in this figure legend, the reader is referred to the web version of this article.)

downstream ('b' in Fig. 14) remains beheaded. Similar sharp anomalous diversions occur at the streams on the right side of the Crati valley, indicated as 'c' and 'd' in Fig. 14. In this case, the upstreams have a flow direction parallel to that of the nearby streams (toward NE) and the sharp turns (toward NW) seem to be controlled mainly from the pull of the deep Crati valley.

Considering this setting along with the other pieces of evidence for the SFZ discussed above, it adds to the definition of a strict interaction between the SFZ, the Crati River valley, and the local drainage pattern.

3.3.2. *Marine terraces displacement*

Marine terraces are present and well preserved in the area. They are important geomorphological markers that form during sea-level high-stands and can be observed in areas affected by tectonic uplift. Therefore, flights of uplifted terraces can provide important constraints to evaluate the regional long-term uplift rates as well as to identify short-wavelength local deformations associated with active faults.

The spectacular flight of marine terraces that marks the Ionian coast of Northern Calabria along tens of kilometers has already been studied in the past decades by several investigators (Cucci and Cinti, 1998; Cucci, 2004, 2005; Ferranti et al., 2009; Santoro et al., 2009, 2013; Lucà et al., 2022; Alfonsi et al., 2023).

Common results from these studies can be summarized as follows: a) the onset of the uplift is set at Middle Pleistocene (~ 0.6 ka); b) the average uplift rates are in the range 0.7–1.0 mm/yr; c) a general northeastward tilt of the whole region occurs with tilt rates in the range 3–6 × 10–3 m km-1 ka-1; d) the terraces record local deformations associated with normal and transpressional faults located north of the study area; e) no evidence of local, fault-induced deformation was found in the area of this study (Cucci, 2004; Ferranti et al., 2009; Santoro et al., 2009). By taking advantage of modern digital tools for terrace analysis, Alfonsi et al. (2023) mapped in the study area (Fig. 2) a flight of seven terraces at elevations ranging between 40 and 360 m asl (± 0.15 m altimetric accuracy, ± 0.30 m planimetric accuracy; Fig. 15). The Authors find that sustained uplift at rates between 0.9 mm/yr and 1.1 mm/yr affected the three lowermost terraces during the past 124 kyrs, and possibly the whole flight of terraces during the past 400 kyrs.

We carefully analyzed the marine terrace setting in Alfonsi et al.

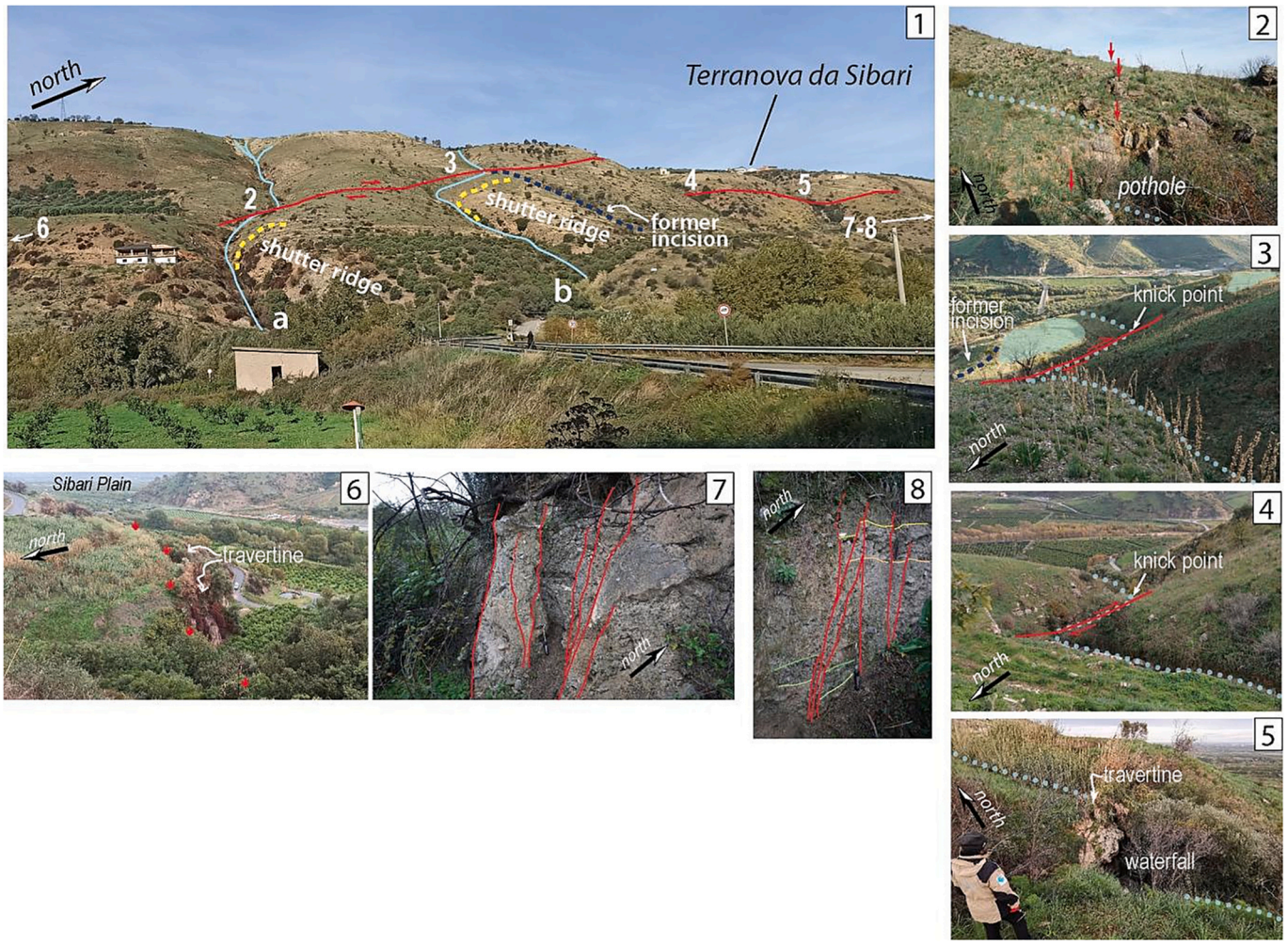

Fig. 11. 1) view of the SE hill slope of Terranova da Sibari with offset streams (letters 'a' and 'b' refer to the streams detailed in Fig. 13) and the schematic trace of the SFZ (red line); numbers locate the photos shown in the other panels. Photos 2 to 5 show details of horizontal and vertical displacement of the streams: 2) arrows indicate the location of the fault (in the background the saddle slope change), light blue line indicates the direction of the displaced streams, the location of a pothole is also shown; 3) dotted line marks the stream cut laterally deflected by the fault, dashed black line indicates the former talweg of the stream flow, the presence of the knick point indicates the vertical displacement. The blue patches are the T4 terrace remnant dismantled by the fault; 4) stream deflected by the fault, symbols as in 3; 5) waterfall and travertine cover (yellow dot#2 in Fig. 10) across the fault line enhancing the vertical component of the fault slip; 6) travertine deposits along the fault line (yellow dot#1 in Fig. 10); 7–8) Grotte site, outcrops of sheared fault zone juxtaposing Pleistocene marine deposits and fluvial conglomerates (see Fig. 10 for location). See also Figs. S3 and S4 in the Supporting Material for additional views of the fault zone features. (For interpretation of the references to colour in this figure legend, the reader is referred to the web version of this article.)

(2023) and found that some of the terraces are affected by local tectonic deformation. Fig. 15a shows that the paleoshorelines form a ~ 2 km-wide embayment across the Crati valley, indicating a paleogulf that originated at least 124 ka ago. Within this paleogulf, sharp anomalies in terraces elevation are observed on the left side of the Crati River (NW sector, Figs. 15 and 16). In this area, terraces T2 and T3, that are well defined as their inner edges are clearly recognized (Fig. 15b), are vertically displaced by about 16 m and 22 m, respectively, over a ~ 2 km horizontal distance (Figs. 16 and 17). Also, two adjacent (<50 m apart) remnants of the T4 wave-cut platform are vertically displaced by about 20 m.

It is noticeable that these anomalies have comparable values and occur across the SFZ near the stream deflections (Fig. 15b).

4. Discussion and conclusions

Archaeological, geophysical, geological, and geomorphological surveys were carried out on the Sibari plain to collect more clues to define the SFZ (initially recognized by Cinti et al., 2015a), its length, geometry, and kinematics. The SFZ was traced as the envelope of several direct and indirect pieces of evidence resulting in an oblique normal-dextral fault zone, ~NE-SW oriented, extending for a length of about 18 km from the Ionian coastline to Terranova da Sibari (Figs. 2 and 18). Fig. 18 represents the SFZ within the regional tectonics. This fault acts in a key zone connecting the extensional (internal sector - west) and the compressive regions (external sector - east) under an E-W to ENE-WSW maximum horizontal stress.

The fault zone is composed of subparallel and locally en-echelon traces occurring in a maximum 500 m wide band, running at different elevations across hills and flat lands. The long-term activity of the SFZ left signatures on the morphology and on the drainage setting of the area, and produced faulting of alluvial deposits, marine terraces, drainage incisions, and on the archaeological structures of *Sybaris*. On the basis of the age of displaced deposits and morphologies, the SFZ shows evidence for activity since at least the Middle-Upper Pleistocene.

We calculated the average slip rate along the SFZ based on the ages and on the accumulated displacements of offset streams and marine terraces (e.g., Molnar and Tapponnier, 1978; Weldon and Sieh, 1985). The T2, T3 and T4 terraces are vertically displaced across the SFZ by an amount of 16 m, 22 m and 20 m, respectively (see also Fig. 16). On the

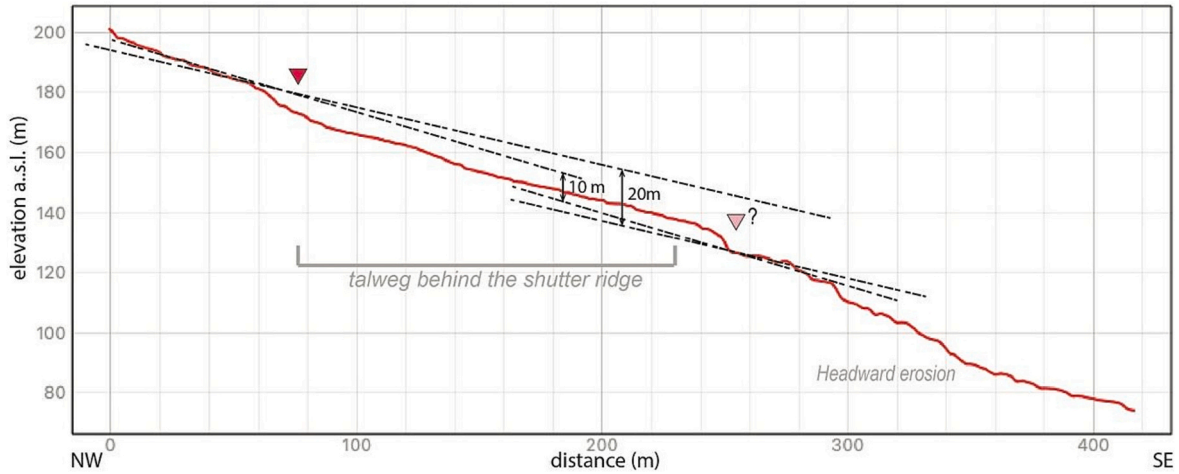

Fig. 12. Topographic profile along the talweg of the offset stream ('b' in Figs. 10 and 11) derived from 0.5 m-DTM obtained by LiDAR survey (horizontal and vertical precision 10 and 5 cm, respectively). Triangles indicate the fault location and the closeby knick-point. The upper part of the talweg bottom (m 0–290) appears quite regular and planar and displaced by the fault strands. Typical headward erosion affects the downstream channel (m 300–400), which is related to the interaction between the tectonic motion and the relative lowering of the basal level represented by the nearby Crati River to the SE. Two possible reconstructions of the talweg bottom across the fault zone with the relative vertical displacement are shown (black dashed lines and vertical arrows, respectively).

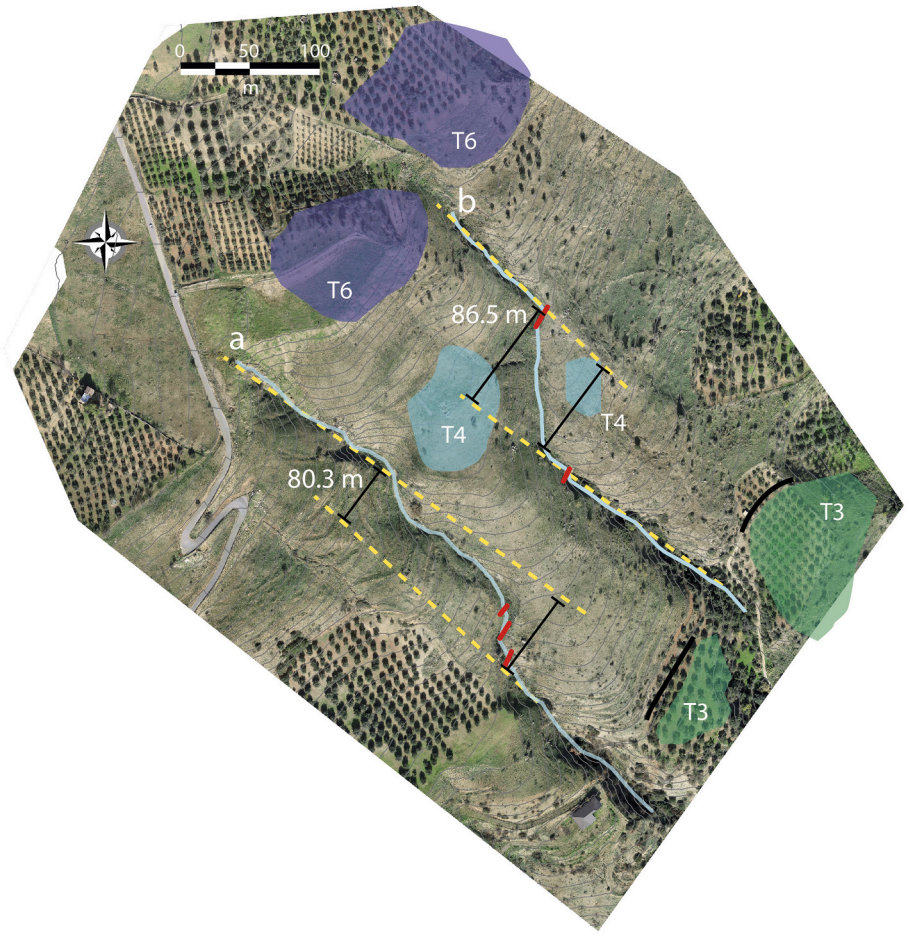

Fig. 13. Orthophoto from drone images acquisition (UAV survey with a 20 megapixel camera) of streams channels 'a' and 'b' showing dextral deflections (see Figs. 10 and 11 for location). Yellow dashed lines indicate the possible projections of the incisions across the fault zone. Red lines locate the fault outcrops within the channels. Remnants of the surfaces of marine terraces T3-T4-T6 are also shown with different colors (see chapter 3.3.2). 5 m contour lines overlay. (For interpretation of the references to colour in this figure legend, the reader is referred to the web version of this article.)

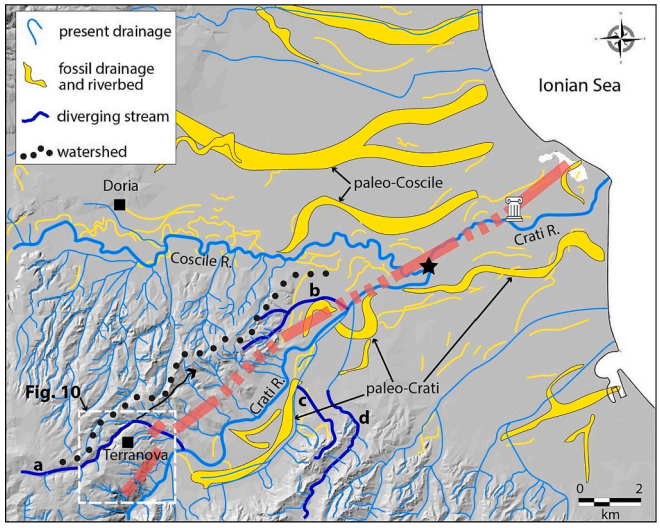

Fig. 14. Present and abandoned drainage pattern in the Sibari Plain (modified from Guerricchio and Melidoro, 1975 and Bellotti et al., 2009). Thick blue lines highlight drainages with anomalous patterns (streams 'a', 'b', 'c', and 'd', see chapter 3.2.1). A black line with an arrow marks an abandoned drainage incision NE of Terranova da Sibari. A star marks the present day confluence of the Crati and Coscile Rivers (since the end of 18th cent., Rizzi Zannoni, 1808). Red bands mark the pattern of the SFZ (see also Fig. 2). The column indicates the location of the *Sybaris* archaeological area; the dashed square corresponds to the area of Fig. 10 (zone 2). Hydrographic network from Regione Calabria (http://geoportale.regione.calabria.it/). (For interpretation of the references to colour in this figure legend, the reader is referred to the web version of this article.)

basis of the chronological attribution of T2, T3 and T4 to 101, 124, and 195 ka, respectively (Alfonsi et al., 2023), we can calculate a local vertical displacement rate of 0.16, 0.18, and 0.10 mm/yr, with the latter value affected by larger uncertainty due to the lack of the terrace inner edge (see chapter 3.3.2).

Horizontal offsets of the SFZ of 80.3 m and 86.5 m were measured on offset streams at Terranova da Sibari (Fig. 13). We assume that the subaerial drainage erosion took place soon after the emergence of the terraced surfaces mapped nearby the offset zone. Thus, we can infer a rough dextral minimum slip rate of 0.41–0.44 mm/yr using the age of T4 (195 kyrs), and 0.65–0.70 mm/yr using terrace T3 (124 kyr). Following the same rationale and considering the 10–20 m of vertical component of the offset streams across the fault zone (Fig. 12), we estimate a vertical slip rate ranging between 0.05 and 0.10 mm/yr (using the age of T4), and 0.08–0.16 (using the age of T3). These estimates compare well to those inferred from the vertical dislocation of the marine terraces (~0.10 to 0.18 mm/yr) and indicate that dextral strike-slip rates are around 3–5 times larger than the dip slip ones, at least in the investigated time window.

Given the 18 km-fault length, and assuming a seismogenic behavior, the SFZ is a primary earthquake source possibly producing moderate to large earthquakes ($M \geq 6$) (Wells and Coppersmith, 1994; Leonard, 2010). On the basis of the available set of data we can also speculate about the recurrence for surface faulting events along the SFZ. Assuming that the ~30 cm of lateral slip measured by Cinti et al. (2015a) on the archaeological structures of *Sybaris* can be considered a minimum slip per event for the whole fault extension (measured on a single fault strand and on manmade structures), and given the dextral slip rates (0.4–0.7 mm/yr), we estimate a minimum average recurrence for surface faulting events of about 700 yrs. This estimate is also in agreement with the ~1000 yrs. recurrence obtained by calculating the expected slip per event from empirical relations (AD vs. SRL, Wells and Coppersmith, 1994) for a fault length of ~18 km (i.e., ~0.4 m) and using the same dextral slip rates. The age of the most recent surface faulting earthquake occurred on the SFZ dated at the ancient *Sybaris* is 1300–1100 yrs. ago, highlighting that the elapsed time approaches the estimated average recurrence.

Finally, this work strengthens the role of high resolution mapping and multidisciplinary approaches for the definition of active faults. It represents a first comprehensive view of the Sibari fault, revealing the extent of the brittle deformation zone and its recent activity. The fault zone that we traced (Figs. 2 and 18) represents the envelope of multiple

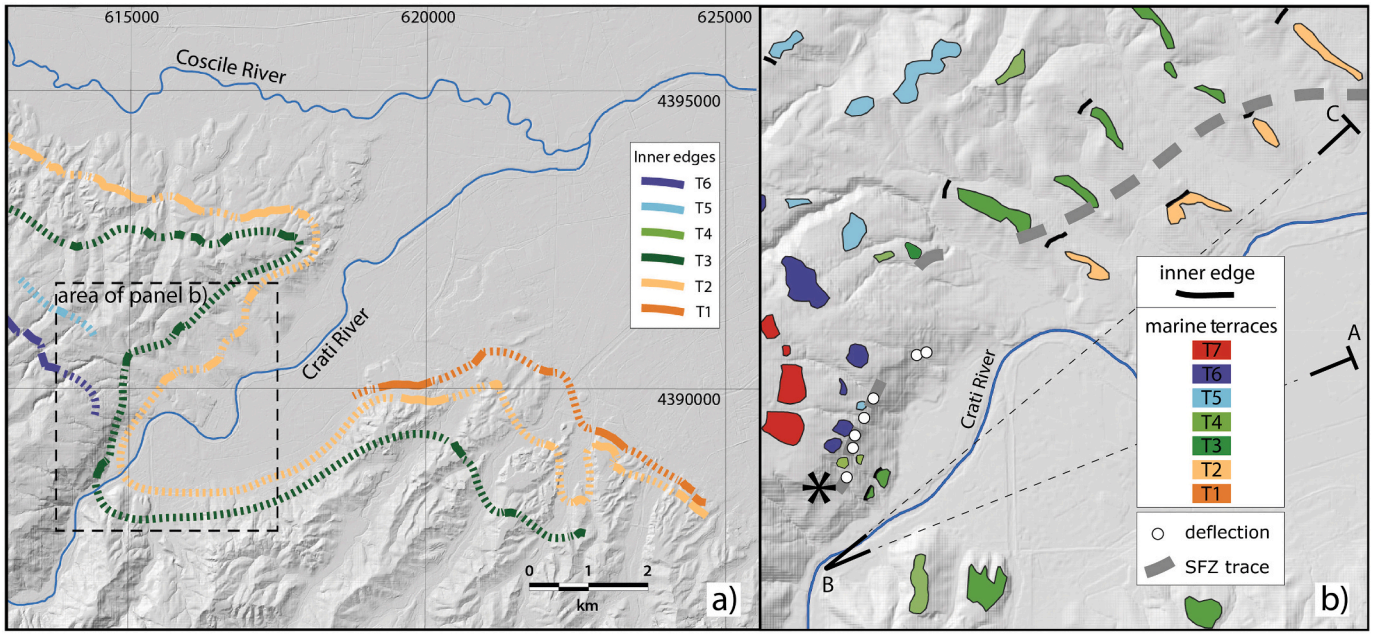

Fig. 15. a) Map of the inner margins of Quaternary marine terraces along the southern side of the Sibari Plain, they highlight the presence of a narrow engulfment along the Crati valley. The contour of the paleoshorelines is dashed when inferred (modified from Alfonsi et al., 2023). b) Detail of the mapped marine terraces near Terranova da Sibari (location in the dashed rectangle in panel a). White circles indicate the location of the drainage deflections, travertines, waterfalls etc. (Section 3.2.1); the asterisk indicates the photo shot point of Fig. 17. Letters A, B, C in panel b) indicate the traces of the transect shown in Fig. 16.

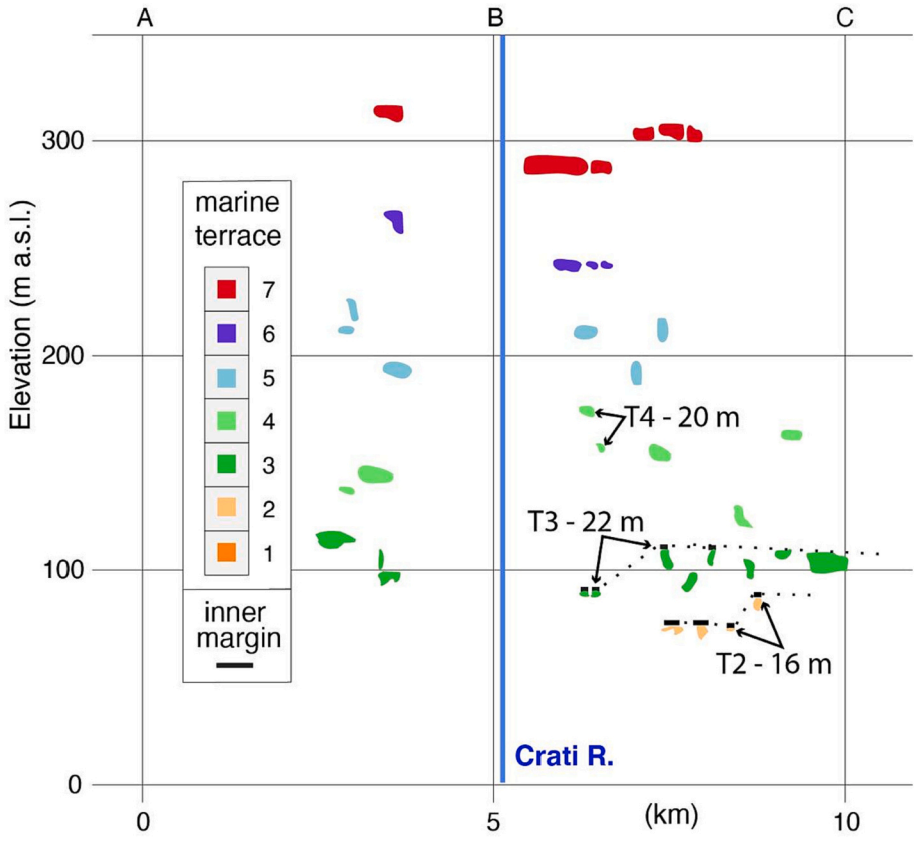

Fig. 16. Marine terrace distribution along coastlines vs elevation along the transect A-B-C (see trace in 15b for location). Arrows indicate offset terraces and amount of displacement. The blue line locates the present position of the Crati River. Please note that the seemingly contradicting sense of motion of T4 relative to T2 and T3 is a graphic outlier due to the direction of projection along the transect. (For interpretation of the references to colour in this figure legend, the reader is referred to the web version of this article.)

Fig. 17. Panoramic view looking East from Terranova da Sibari. Pink and orange patches mark the outcrops of the T2 and T3 marine terraces, respectively. White arrows indicate the amount of vertical displacement observed for T2 and T3 across the SFZ trace (dashed red line). (For interpretation of the references to colour in this figure legend, the reader is referred to the web version of this article.)

individual observations and clues that can be further enriched through future studies.

In light of these results, the SFZ should be included among the faults that contain a potential seismic hazard in this poorly known portion of the Ionian sector of northern Calabria.

CRediT authorship contribution statement

F.R. Cinti: Writing – review & editing, Writing – original draft, Visualization, Validation, Supervision, Methodology, Investigation, Formal analysis, Data curation, Conceptualization. **L. Alfonsi:** Writing – original draft, Visualization, Validation, Methodology, Investigation, Formal analysis, Data curation, Conceptualization. **L. Cucci:** Writing – original draft, Visualization, Validation, Supervision, Methodology, Investigation, Formal analysis, Data curation, Conceptualization. **D. Pantosti:** Writing – original draft, Visualization, Validation, Supervision, Methodology, Investigation, Formal analysis, Data curation, Conceptualization. **C. Pauselli:** Writing – review & editing, Writing – original draft, Validation, Methodology, Investigation, Data curation. **M. Ercoli:** Writing – review & editing, Writing – original draft, Validation, Investigation, Data curation, Conceptualization. **C.A. Brunori:** Writing – original draft, Validation, Methodology, Investigation, Data curation, Conceptualization. **G. Cianflone:** Writing – review & editing, Writing – original draft, Validation, Software, Methodology, Investigation, Data curation. **R. Dominici:** Writing – review & editing, Writing – original draft, Validation, Methodology, Investigation, Data curation.

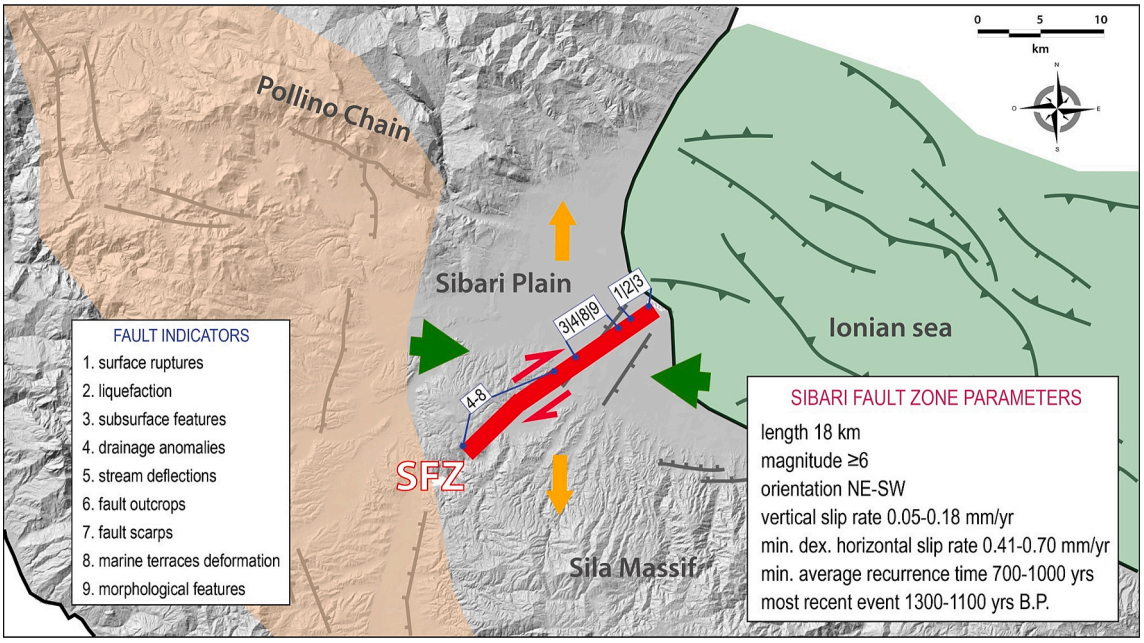

Fig. 18. The SFZ in the regional tectonics. Green and orange arrows indicate the compressional and extensional stress directions in the SFZ sector. Light orange area encloses the internal region with extensional regime, and the light green area is the external offshore region under compression. Inset to the right summarizes the preliminary main SFZ parameters. We also display the different fault indicators (1 to 9 in the inset to the left) that once integrated lead to the recognition of the SFZ. (For interpretation of the references to colour in this figure legend, the reader is referred to the web version of this article.)

Declaration of competing interest

The authors declare that they have no known competing financial interests or personal relationships that could have appeared to influence the work reported in this paper.

Data availability

Data will be made available on request.

Acknowledgements

We want to thank the anonymous reviewers for their thoughtful comments and suggestions helping us to prepare an improved version of our work. Part of the research at the archaeological site of Sybaris was conducted under the frame of the DPC project S1 - Base-knowledge improvement for assessing the seismogenic potential of Italy 2014-2015. Report DPC-INGV-S1 Project" Base-knowledge improvement for assessing the seismogenic potential of Italy". This study benefited from the fruitful collaboration with the local archaeological authorities, dr. A. D'Alessio (former Directors of the Parco Archeologico e Museo di Sibari) and dr. S. Marino (former Officer of Soprintendenza per i Beni Archeologici della Calabria) and from the fruitful discussion with dr. Annalisa Correale (archaeologist of Scuola Archeologica Italiana di Atene). The authors wish to acknowledge Mr. Leonardo Speziali for the logistical support, Dr. Massimiliano Mazzocca (GeoPro) and Dr. Andrea Fucelli for ERT data acquisition and processing, Prof. Costanzo Federico for the help during the GPR fieldwork and Dr. Roberto Volpe for his support during GPR data organization and processing. The authors also thank the Laboratorio Marino SILA (Università della Calabria) for support during the drone survey.

Appendix A. Supplementary data

Supplementary data to this article can be found online at https://doi.org/10.1016/j.tecto.2024.230214.

References

Alfonsi, L., Brunori, C.A., Cucci, L., 2023. Mapping and chronological classification of marine terraces along the southern side of the Sibari Plain (northern Calabria, Italy) by means of digital and analogue tools. J. Maps 19, 1. https://doi.org/10.1080/17445647.2023.2243983.

Amoroso, N., Cilli, R., Nitti, D.O., Nutricato, R., Iban, M.C., Maggipinto, T., Tangaro, S., Monaco, A., Bellotti, R., 2023. PSI Spatially Constrained Clustering: the Sibari and Metaponto Coastal Plains. Remote Sens. (Basel) 15 (10), 2560. https://doi.org/10.3390/rs15102560.

Bellotti, P., Caputo, C., Dell'Aglio, P.L., Davoli, L., Ferrari, K., 2009. Insediamenti urbani in un paesaggio in evoluzione: interazione uomo-ambiente nella Piana di Sibari (Calabria ionica). Il Quat. Ital. J. Quat. Sci. 22 (1), 61–72.

Stanley, J.-D., Bernasconi, M.P., 2009. Sybaris-Thuri-Copia trilogy: three delta coastal sites become land-locked. Méditerranée 112, 75–86. https://doi.org/10.4000/mediterranee.3190.

Brozzetti, F., Cirillo, D., de Nardis, R., Cardinali, M., Lavecchia, G., Orecchio, B., Presti, D., Totaro, C., 2017a. Newly identified active faults in the Pollino seismic gap, southern Italy, and their seismotectonic significance. J. Struct. Geol. 94, 13–31. https://doi.org/10.1016/j.jsg.2016.10.005.

Brozzetti, F., Cirillo, D., Liberi, F., Piluso, E., Faraca, E., de Nardis, R., Lavecchia, G., 2017b. Structural style of Quaternary extension in the Crati Valley (Calabrian Arc): evidence in support of an east-dipping detachment fault. Italian J. Geosci. 136 (3), 434–453.

Cianflone, G., Tolomei, C., Brunori, C.A., Dominici, R., 2015. InSAR time series analysis of natural and anthropogenic coastal plain subsidence: the case of Sibari (Southern Italy). Remote Sens. (Basel) 7, 16004–16023.

Cianflone, G., Cavuoto, G.B., Punzo, M., Dominici, R., Sonnino, M., Di Fiore, V., Pelosi, N., Tarallo, D., Lirer, F., Marsella, E., Critelli, S., De Rosa, R., 2018. Late quaternary stratigraphic setting of the Sibari Plain (southern Italy): Hydrogeological implications. Mar. Petrol. Geol. 97, 422–436.

Cinti, F.R., Cucci, L., Pantosti, D., D'Addezio, G., Meghraoui, M., 1997. A Major seismogenic fault in a "silent area": the Castrovillari fault (southern Apennines, Italy). Geophys. J. Int. 130, 595–605. https://doi.org/10.1111/j.1365-246X.1997.tb01855.X.

Cinti, F.R., Moro, M., Pantosti, D., Cucci, L., D'Addezio, G., 2002. New constraints on the seismic history of the Castrovillari fault in the Pollino gap (Calabria, southern Italy). J. Seism. 6, 199–217. https://doi.org/10.1023/A:1015693127008.

Cinti, F.R., Alfonsi, L., D'Alessio, A., Marino, S., Brunori, C.A., 2015a. Faulting and Ancient Earthquakes at Sybaris Archaeological Site, Ionian Calabria, Southern Italy. Seismological Research Letters 86, 1. https://doi.org/10.1785/02201401071.

Cinti, F.R., Pauselli, C., Livio, F., Ercoli, M., Brunori, C.A., Ferrario, F., Volpe, R., Civico, R., Pantosti, D., Pinzi, S., De Martini, P.M., Ventura, G., Alfonsi, L., Gambillara, R., Michetti, A.M., 2015b. Integrating multidisciplinary, multi-scale geological and geophysical data to image the Castrovillari fault (Northern Calabria, Italy). Geophys. J. Int. 203, 1847–1863. https://doi.org/10.1093/gji/ggv404.

Cirillo, D., Totaro, C., Lavecchia, G., Orecchio, B., de Nardis, R., Presti, D., et al., 2022. Structural complexities and tectonic barriers controlling recent seismic activity in

the Pollino area (Calabria–Lucania, southern Italy) – constraints from stress inversion and 3D fault model building. Solid Earth. 13, 205–228. https://doi.org/10.5194/se-13-205-2022.
Cucci, L., 2004. Raised marine terraces in the Northern Calabrian Arc (Southern Italy): a ~600 kyr-long geological record of regional uplift. Ann. Geophys. 47 (4), 1391–1406.
Cucci, L., 2005. Geology versus myth: the Holocene evolution of the Sybaris plain. Ann. Geophys. 48, 1017–1033.
Cucci, L., Cinti, F.R., 1998. Regional uplift and local tectonic deformation recorded by the Quaternary marine terraces on the Ionian coast of northern Calabria (southern Italy). Tectonophysics 292 (1998), 67–83.
D'Agostino, N., D'Anastasio, E., Gervasi, A., Guerra, I., Nedimovic, M.R., Seeber, L., et al., 2011. Forearc extension and slow rollback of the Calabrian Arc from GPS measurements. Geophys. Res. Lett. 38 (17) https://doi.org/10.1029/2011GL048270.
De Gori, P., Lucente, F.P., Govoni, A., Margheriti, L., Chiarabba, C., 2022. Seismic swarms in the Pollino seismic gap: positive fault inversion within a popup structure. Front. Earth Sci. 10, 968187 https://doi.org/10.3389/feart.2022.968187.
Del Ben, A., Barnaba, C., Taboga, A., 2008. Strike-slip systems as the main tectonic features in the Plio-Quaternary kinematics of the Calabrian Arc. Mar. Geophys. Res. 29, 1–12. https://doi.org/10.1007/s11001-007-9041-6.
Ercoli, M., Pauselli, C., Forte, E., Di Matteo, L., Mazzocca, M., Frigeri, A., Federico, C., 2012. A multidisciplinary geological & geophysical approach to define structural and hydrogeological implications of the Molinaccio spring (Spello, Italy). J. Appl. Geophys. 77, 72–82.
Faccenna, C., Becker, T.W., Lucente, F.P., Jolivet, L., Rossetti, F., 2001. History of subduction and back-arc extension in the Central Mediterranean. Geophys. J. Int. 145, 809–820. https://doi.org/10.1046/j.0956-540x.2001.01435.x.
Ferranti, L., Santoro, E., Mazzella, M.E., Monaco, C., Morelli, D., 2009. Active transpression in the northern Calabria Apennines, southern Italy. Tectonophysics 476 (2009), 226–251.
Ferranti, L., Pagliarulo, R., Antonioli, F., Randisi, A., 2011. Punishment for the sinner: Holocene episodic subsidence and steady tectonic motion at ancient Sybaris (Calabria, southern Italy). Quat. Int. 232 (2011), 56–70.
Ferranti, L., Burrato, P., Pepe, F., Santoro, E., Mazzella, M.E., Morelli, D., Passaro, S., Vannucci, G., 2014. An active oblique contractional belt at the transition between the Southern Apennines and Calabrian Arc: the Amendolara Ridge, Ionian Sea, Italy. Tectonics 33, 2169–2194. https://doi.org/10.1002/2014TC003624.
Ferranti, L., Pace, B., Valentini, A., Montagna, P., Pons-Branchu, E., Tisnérat-Laborde, N., Maschio, L., 2019. Speleoseismological constraints on ground shaking threshold and seismogenic sources in the Pollino Range (Calabria, southern Italy). J. Geophys. Res. Solid Earth 124, 5192–5216. https://doi.org/10.1029/2018JB01700.
Frepoli, A., Amato, A., 2000. Spatial variation in stresses in peninsular Italy and Sicily from background seismicity. Tectonophysics 317 (1–2), 109–124.
Frepoli, A., Maggi, C., Cimini, G.B., Marchetti, A., Chiappini, M., 2011. Seismotectonic of Southern Apennines from recent passive seismic experiments. J. Geodyn. 51 (2–3), 110–124. https://doi.org/10.1016/j.jog.2010.02.007.
Galli, P., Spina, V., Ilardo, I., Naso, G., 2010. Evidence of active tectonics in southern Italy: The Rossano fault (Calabria). In: Guarnieri, P. (Ed.), Recent Progress on Earthquake Geology. Nova Science Publishers, pp. 49–78.
Greco, E., 2017. Annuario della Scuola archeologica di Atene e delle Missioni italiane in Oriente. Volume XCIV, Serie III, 16 2016. SAIA, p. 2017.
Guerricchio, G., Melidoro, G., 1975. Ricerche di geologia applicata all'archeologia della città di Sibari sepolta. Geol. Appl. Idrogeol. 10, 107–128.
ISIDe Working Group, 2007. Italian Seismological Instrumental and Parametric Database (ISIDe). Istituto Nazionale di Geofisica e Vulcanologia (INGV). https://doi.org/10.13127/ISIDE.
Kagan, E.J., Cinti, F.R., Alfonsi, L., Civico, R., Bar-matthews, M., 2017. Broken speleothems reveal Holocene and late Pleistocene paleoearthquakes in Northern Calabria, Italy. Quat. Int. 451, 176–184. https://doi.org/10.1016/j.quaint.2016.10.023.
Lanzafame, G., Tortorici, L., 1981. La tettonica recente della Valle del Fiume Crati (Calabria). Geogr. Fis. Dinam. Quat. 4, 11–22.
Lena, G., Osso, G., Orsino, L., 2021. Variazioni della linea di costa lungo la catena costiera calabrese. Analisi della cartografia storica e dei dati geomorfologici. Mem. Descr. Carta Geol. d'It. 108, 83–106 (figg. 34).
Leonard, M., 2010. Earthquake Fault Scaling: Self-Consistent Relating of Rupture Length, Width, Average Displacement, and Moment Release. Bull. Seism. Soc. Am. 100 (5A), 1971–1988. https://doi.org/10.1785/0120090189.
Lucà, F., Brogno, A., Tripodi, V., Robustelli, G., 2022. Terrace Morpho-Sedimentary Sequences on the Sibari Plain (Calabria, Southern Italy): Implication for Sea Level and Tectonic Controls. Geosciences 12, 211. https://doi.org/10.3390/geosciences12050211.
Mariucci, M.T., Montone, P., 2022. IPSI 1.5, Database of Italian Present-day Stress Indicators, Istituto Nazionale di Geofisica e Vulcanologia (INGV). https://doi.org/10.13127/IPSI.1.5.
Michetti, A.M., Ferreli, L., Serva, L., Vittori, E., 1997. Geological evidence for strong historical earthquakes in an "aseismic" region: the Pollino case (Southern Italy). J. Geodyn. 24, 67–86.
Molnar, P., Tapponnier, P., 1978. Active tectonics of Tibet. J. Geophys. Res.: Solid Earth 83 (B11), 5361–5375.
Napolitano, F., Amoroso, O., La Rocca, M., Gervasi, A., Gabrielli, S., Capuano, P., 2021. Crustal structure of the seismogenic volume of the 2010–2014 Pollino (Italy) seismic sequence from 3D P-and S-wave tomographic images. Front. Earth Sci. (Lausanne). 9 https://doi.org/10.3389/feart.2021.735340.
Pondrelli, S., Salimbeni, S., Ekström, G., Morelli, A., Gasperini, P., Vannucci, G., 2006. The Italian CMT dataset from 1977 to the present. Phys. Earth Planet. In. 159 (3/4), 286–303. https://doi.org/10.1016/j.pepi.2006.07.008.
Quye-Sawyer, J., Whittaker, A.C., Roberts, G.G., Rood, D.H., 2021. Fault throw and regional uplift histories from drainage analysis: Evolution of Southern Italy. Tectonics 40, e2020TC006076. https://doi.org/10.1029/2020TC006076.
Rizzi Zannoni, G.A., 1808. Atlante Geografico del Regno di Napoli compito e rettificato sotto i felici auspicj di Giuseppe Napoleone I re di Napoli e di Sicilia (tavola 26, Calabria Citra), Napoli.
Rovida, A., Locati, M., Camassi, R., Lolli, B., Gasperini, P., Antonucci, A., 2022. Italian Parametric Earthquake Catalogue (CPTI15), version 4.0. Istituto Nazionale di Geofisica e Vulcanologia (INGV). https://doi.org/10.13127/CPTI/CPTI15.4.
Santoro, E., Mazzella, M.E., Ferranti, L., Randisi, A., Napolitano, E., Rittner, S., Radtke, U., 2009. Raised coastal terraces along the Ionian Sea coast of northern Calabria, Italy, suggest space and time variability of tectonic uplift rates. Quat. Int. 206, 78–101.
Santoro, E., Ferranti, L., Burrato, P., Mazzella, M.E., Monaco, C., 2013. Deformed Pleistocene marine terraces along the Ionian Sea margin of southern Italy: Unveiling blind fault-related folds contribution to coastal uplift. Tectonics 32I (3), 737–762.
Scognamiglio, L., Tinti, E., Quintiliani, M., 2006. Time Domain Moment Tensor (TDMT) [Data set]. In: Istituto Nazionale di Geofisica e Vulcanologia (INGV). https://doi.org/10.13127/TDMT.
Tansi, C., Muto, F., Critelli, S., Iovine, G., 2007. Neogene–Quaternary strike-slip tectonics in the central Calabrian Arc (southern Italy). J. Geodyn. 43, 393–414.
Tertulliani, A., Cucci, L., 2014. New insights on the strongest historical earthquake in the Pollino region (southern Italy). Seismol. Res. Lett. 85 (3), 743–751. https://doi.org/10.1785/0220130217.
Van Dijk, J.P., Bello, M., Brancaleoni, G.P., Cantarella, G., Costa, V., Frixa, A., Golfetto, F., Merlini, S., Riva, M., Torricelli, S., Toscano, C., Zerilli, A., 2000. A regional structural model for the northern sector of the Calabrian Arc (southern Italy). Tectonophysics 324, 267–320.
Vannucci, G., Gasperini, P., 2004. The New Release of the Database of earthquake Mechanisms of the Mediterranean Area (EMMA Version 2). Ann. Geophys. 47, 303–327.
Weldon, R.J., Sieh, K.E., 1985. Holocene rate of slip and tentative recurrence interval for large earthquakes on the San Andreas fault, Cajon Pass, southern California. Geol. Soc. Am. Bull. 96 (6), 793–812.
Wells, D.L., Coppersmith, K.J., 1994. New empirical relationships among magnitude, rupture length, rupture width, rupture area, and surface displacement. Bull. Seismol. Soc. Am. 84 (4), 974–1002.
Zecchi, R., Giorgi, G., Francavilla, F., Ronchi, A., 2003. Tendenze evolutive recenti del delta del fiume Crati (Calabria-Italy) sulla base della cartografia storica e delle immagini telerilevate. In: Atti 7° Conferenza Nazionale ASITA, Verona 2003 (on line). http://www.asita.it.